JPhys Energy

TOPICAL REVIEW • OPEN ACCESS

Recent progress in 3D printing of Bi_2Te_3-based thermoelectric materials and devices

IOP Publishing J. Phys. Energy 6 (2024) 022003 https://doi.org/10.1088/2515-7655/ad3983

Journal of Physics: Energy

TOPICAL REVIEW

Recent progress in 3D printing of Bi_2Te_3-based thermoelectric materials and devices

S E Yang[1], H Han[1] and J S Son[2,*]

[1] Department of Materials Science and Engineering, Ulsan National Institute of Science and Technology (UNIST), Ulsan 44919, Republic of Korea
[2] Department of Chemical Engineering, Pohang University of Science and Technology (POSTECH), Gyeongsangbuk-do 37673, Republic of Korea
* Author to whom any correspondence should be addressed.

E-mail: sonjs@postech.ac.kr

Keywords: 3d printing, thermoelectrics, Bi_2Te_3, BiSbTe, power generator

OPEN ACCESS

RECEIVED
10 October 2023

REVISED
24 January 2024

ACCEPTED FOR PUBLICATION
2 April 2024

PUBLISHED
12 April 2024

Abstract

With growing concerns about the depletion of fossil fuels and climate change, there is an urgent global demand for the development of sustainable and renewable energy sources. The thermoelectric technology, which converts waste heat into electricity, presents a unique opportunity to ensure a sustainable electric supply and enhance energy efficiency without incurring additional costs. Recently, the utilization of three-dimensional (3D) printing technology for fabricating thermoelectric materials has attracted tremendous interest because of the simplicity of design of power generators and the potential for economical manufacturing. This study focuses on research related to Bi_2Te_3 thermoelectric materials produced using 3D printing, and it highlights the fundamental principles, advantages, challenges, and recent remarkable advancements associated with this manufacturing approach. Furthermore, we explored various device applications, including shape-conformable wearable, and micro devices with printed thermoelectric materials. Finally, we discuss the promising research directions and prospects for industrialization in 3D-printed thermoelectric materials.

1. Introduction

Global energy demand is steadily on the rise, with fossil fuels dominating the global energy consumption [1, 2]. Ongoing concerns about climate change and the depletion of fossil fuel have made the transition to a sustainable energy system imperative. Waste heat is one of the most prominent renewable energy sources in the industrial and transportation sectors, as approximately 66% of the total energy usage is dissipated in the form of waste heat [3]. Thus, recovering even a fraction of waste heat would enhance energy usage efficiency at no additional costs. Accordingly, thermoelectric (TE) energy conversion has attracted tremendous attention owing to its capability to convert waste heat directly into electricity, which enhances economic benefits, reduces dependence on fossil fuels, and lowers greenhouse gas emissions [4, 5].

The efficiency of the TE generator (TEG) can be expressed according to the following equation [6]:

$$\eta = \frac{\Delta T}{T_H}\frac{\sqrt{1+ZT}-1}{\sqrt{1+ZT}+\frac{T_C}{T_H}},$$

which is a function of the dimensionless figure of merit (ZT) and ΔT as the imposed temperature difference; T_H and T_C are the temperatures of the hot side and cold side, respectively. The figure of merit is given by $ZT = \sigma S^2 T/\kappa$, where S, σ, T, and κ are the seebeck coefficient, electrical conductivity, absolute temperature, and thermal conductivity, respectively. TE research has mostly focused on improving the material ZT values to enhance efficiency, which is achieved using a range of strategies, including defect engineering, nano structuring, band structure engineering, and entropy engineering [7–18]. Another important strategy for improving the efficiency of the TEG is device engineering, which aims at the thermal design of TE devices to

Table 1. Examples of printing methods and their key characteristics.

Dispenser printing	Fused deposition modeling	Powder bed fusion	Aerosol jet printing	Stereolithography
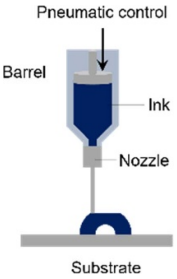	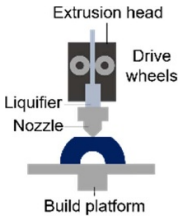	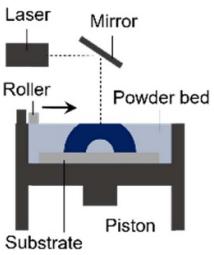	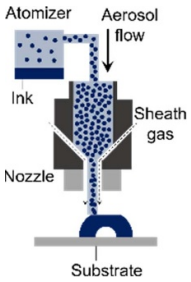	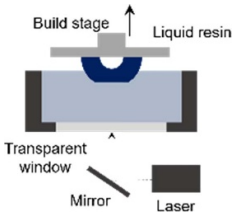
Advantages				
Rapid process, Low cost, Multi-material	Smooth surface, Low initial cost, Flexibility	Low cost, No extra support, Wide materials	High accuracy, Rapid prototyping	High accuracy, Smooth surface
Disadvantages				
Low resolution, Rough surface	Time-consuming, Low resolution,	Post-processing, Time-consuming	Limit of material choices	Post-processing, Time-consuming
Required ink property				
Viscoelasticity	Thermoplastic (filament)	Thermoplastic (powder)	Low viscosity <50 m Pa s	Photocurability Low viscosity <5 Pa s

generate substantial temperature differences [19]. This strategy can include designing a heat sink, modulating interfacial thermal resistances, and optimizing the design parameters for TE legs, all of which require the geometrical customization of TE materials and devices [20–24].

The traditional manufacturing process for TE devices typically begins with the synthesis of ingots using methods such as spark plasma sintering, melt-spinning, zone melting, and ball milling [25–29]. These ingots are subsequently sliced into legs, after which they are planted, cleaned, and assembled onto the metal electrodes of the substrate through soldering [30]. These complex procedures are costly and time-consuming, and they result in substantial material loss during the dicing process [21, 31]. Furthermore, conventional dicing processes restrict TE devices to cuboid geometries, impeding the flexible geometric thermal design of TE legs. To address these constraints in the manufacturing process, increasing attention has been paid to investigating alternative fabrication methods, particularly additive manufacturing [32–38]. A subset of additive manufacturing is three-dimensional (3D) printing technology, which involves constructing 3D objects from digital designs through controlled material deposition in layers [39]. This technology considerably reduces the costs and time associated with design adjustments and production, thereby facilitating rapid prototyping and the creation of complex individual components [40]. 3D printing commonly includes dispenser printing, fused deposition modeling (FDM), powder bed fusion (PBF), aerosol jet printing (AJP), and stereolithography (SLA), each of which has its own advantages and characteristics (table 1) [40, 41].

Although researchers have extensively explored the fabrication of state-of-the-art TE materials (e.g. Bi_2Te_3, PbTe, Cu_2Se, and SnSe) through 3D printing [32, 42–44], this review specifically focuses on research related to Bi_2Te_3. Bi_2Te_3-based materials are widely regarded as the most efficient TE materials for applications under near-room-temperature conditions, and their TE properties for various compositions and structures are well established [45, 46]. In this review, we present an overview of the notable research advancements in Bi_2Te_3 TE materials produced through 3D printing. Our discussion begins by exploring the fundamental principles, advantages, and challenges associated with each technique, emphasizing the

remarkable advancements achieved in recent years. Subsequently, we review diverse device applications of 3D-printed TE materials, including shape-conformal, wearable, and microdevices, as well as thermal management. Finally, we explore promising directions and prospects for the industrialization of printing-related TE materials.

2. 3D printing of Bi_2Te_3-based thermoelectric materials

2.1. Dispenser printing

Dispenser printing, also known as material extrusion or material deposition, is a widely used 3D printing technique that is renowned for its cost-effectiveness, versatility, and applicability in various industries [47]. The process entails precise layer-by-layer material deposition through a nozzle or dispenser head under pneumatic pressure for constructing 3D objects, with the resolution typically determined by the diameter of the printing nozzle [48, 49].

To engage in effective dispenser 3D printing, the use of viscoelastic ink is crucial, as it guarantees the structural stability of the printed layers [50, 51]. The viscoelasticity is generally achieved through the addition of binders, which enhance the viscoelasticity of the ink, and organic materials are typically selected as the binders because of their cost-effectiveness and availability. For instance, Su *et al* [52] used polyvinylpyrrolidone (PVP) as an organic binder, and PVP is widely used in ink formulation because of its excellent viscoelastic properties, nontoxicity, and low melting point (figure 1(a)). A bulk cuboid and a filament were successfully printed by a needle with a diameter of 100 μm, and the filament had a uniform thickness. The printed composites containing 91 wt% TE filler reached peak ZT values of 0.104 (p-type) and 0.11 (n-type). In another study [53], poly-lactic-co-glycolic-acid (PLGA) was used as an organic binder (figure 1(b)). Interestingly, this study involved the fabrication of Bi_2Te_3 material using blended Bi_2O_3 and TeO_2 oxide precursor powders. Oxide precursors eliminate the need for complex pre-alloyed powder production and offer compositional flexibility, cost reduction, and ease of handling. Starting with the presintering of the green oxide body in air, the oxides undergo interdiffusion, leading to the formation of ceramics, including $Bi_2Te_4O_{11}$, $Bi_2Te_2O_7$, and TeO_2. After the co-reduction of the presintered ceramics in an H_2 atmosphere, fine-grained, Te-rich n-type Bi_2Te_3 material was obtained, resulting in a ZT value of 0.4.

Organic binders contribute considerably to ink formulation with suitable rheological properties for dispenser printing [33, 56]. However, they exhibit peculiar limitations owing to their poor electrical properties and markedly lower ZT values compared to those of traditional bulk cuboid samples [52, 57–59]. Moreover, even after the high temperature sintering process, these organic binders decrease the sintering efficiency of inorganic particles, degrading the functional properties of final products. The sintering process is essential to obtain materials with high TE properties and mechanical robustness. To overcome the limitations of organic binders, Kim *et al* [32] developed all-inorganic viscoelastic TE inks, using Sb_2Te_3 chalcogenidometallate (ChaM) ions as inorganic binders (figure 1(c)). The introduction of ChaM ions enhanced the viscoelasticity of the ink, yielding the envisioned 3D printing capabilities, such as tailored shaping and scalability. In addition, ChaM acts as a sintering aid for Bi_2Te_3-based particles by filling up void spaces and facilitating the structural transformation from molecular ions to crystalline phases during heat treatment, leading to the densification of materials. These inks were used to produce TE materials with various shapes like cuboid, disc, and half-ring, and the materials exhibited high TE performance, with ZT values reaching 0.6 and 0.9 for n-type and p-type materials, respectively. Subsequently, Yang *et al* [54] performed sequential multi-material 3D printing by diversifying TE inks containing $Bi_xSb_{2-x}Te_3$ (BST) particles ($x = 0.3$–0.6) with $Sb_2Te_4^{2-}$ ChaM inorganic binders (figure 1(d)). They successfully fabricated a compositionally segmented bulk tri-block TEG, extending the peak ZTs of the TE legs from room temperature up to 250 °C with a high efficiency of 8.7%.

Despite the progress in the development of TE inks, dispenser-printed TE structures still have certain limitations in terms of ink printability, which reduce the functionality and resolution of the printed objects. To overcome these challenges, Kim *et al* [48] investigated super-high viscoelastic TE inks for direct ink writing (DIW) (figure 1(e)). DIW has emerged as the predominant 3D printing technique in energy device manufacturing because of its straightforward operation, cost effectiveness, expansive material choices, and capacity to construct highly accurate and complex 3D structures directly from a digital design [60]. By optimizing the TE particle size, size distribution, and surface states, the authors developed TE inks with extremely high viscoelasticity, creating complex 3D architectures, such as arch-type or scaffold architectures. Recently, Zhang *et al* [55] reported a unique approach to creating complex cellular structures using DIW with thermal ink gelation, which was achieved using Pluronic systems (figure 1(f)). Depending on thermo-reversible liquid-to-gel transition temperature (T_{gel}), the TE ink, which contains $Bi_{0.5}Sb_{1.5}Te_3$ powder within a Pluronic F127 gel matrix, can exist as either a sol or gel when subjected to a particular temperature. At room temperature, it forms a stable gel, and the 3D-BST ink displays shear thinning behavior

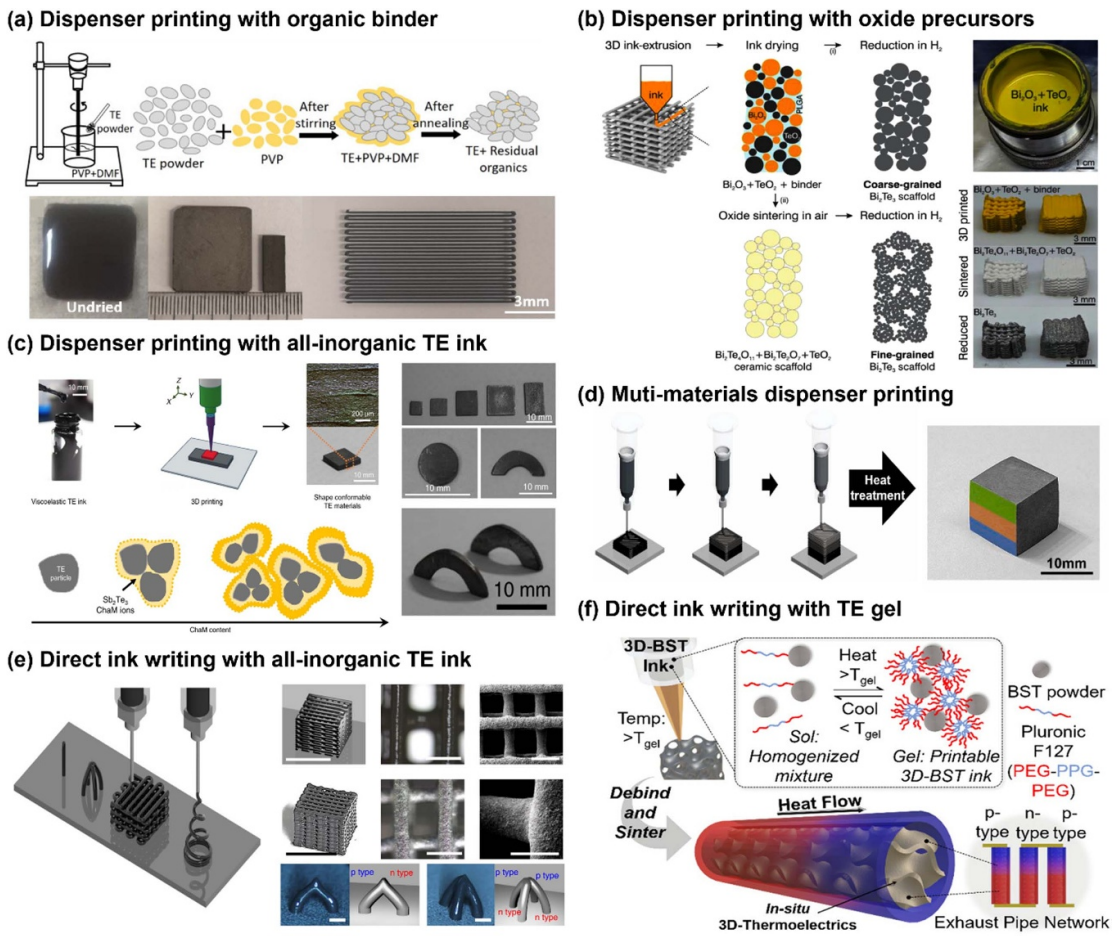

Figure 1. Dispenser printed TE materials. (a) Schematic illustration of the synthetic process of the TE slurry and photographs of the undried and dried samples and a filament printed by a needle with a diameter of 100 mm. Reprinted from [52], Copyright (2020), with permission from Elsevier. (b) Process schematic showing 3D ink extrusion printing of $Bi_2O_3 + TeO_2$ inks and Bi_2Te_3 synthesis. Reprinted from [53], Copyright (2021), with permission from © 2021 Acta Materialia Inc. Published by Elsevier Ltd. All rights reserved. (c) Schematic illustration of an extrusion-based 3D printing process using all-inorganic TE inks and photographs of the printed *p*-type cuboids, disc, and half-ring structures. Reproduced from [32], with permission from Springer Nature. (d) Schematic illustration for multi-material 3D printing of the compositionally segmented TE leg. Reprinted from [54], Copyright (2020), with permission from Elsevier. (e) Schematic illustration of the direct ink writing for 3D TE architectures and photographs of the printed 3D lattice and arch-type architectures. Reproduced from [48], with permission from Springer Nature. (f) Schematic illustration of the direct ink writing for the porous BST gyroid structures for *in situ* waste heat harvesting in an exhaust pipe system. Reprinted with permission from [55]. Copyright (2023) American Chemical Society.

with increasing shear, making it suitable for DIW processes. The sintered hierarchical porous 3D-BST gyroid structure exhibited a maximum *ZT* of 0.187. As numerous TE waste heat recovery applications require TE devices to function on curved surfaces and necessitate geometric TE designs for controlled thermal transport, dispenser printing with TE inks holds great promise for the production of TE generators with diverse shapes.

2.2. Fusion deposition modeling

FDM is a 3D printing technology that involves melting a thermoplastic material into a liquid state and layering it to create 3D objects [61]. It is a cost-effective and versatile manufacturing method that is widely used in diverse industries for prototyping, manufacturing, and fostering creativity [62, 63].

To manufacture TE materials using FDM technology, the development of thermoplastic TE materials is crucial [63]. Several studies have introduced organic polymer binders such as polylactide-co-glycolide (PLG), polyactic acid (PLA) and acrylonitrile-butadienestyrene (ABS) into the composite to improve its thermoplastic properties [33, 64–67]. For example, Peng *et al* [33] reported continuous, flexible TE threads fabricated through rapid 3D-printable composite ink extrusion (figure 2(a)). To synthesize composite 3D paints, the authors blended TE powders dispersed in dichloromethane with a polymer binder (PLG) in a suitable volume ratio. The threads were extruded at a rate of $r = 4$ cm s^{-1} in ambient air and collected using a spool. The electrical properties of the threads were considerably improved when a lateral compression of the threads was achieved through pressure control, resulting in plastic deformation. The *ZT* values of the compressed *p*- and *n*-type threads reached 0.08 and 0.005 at 360 K, respectively. In addition, the threads

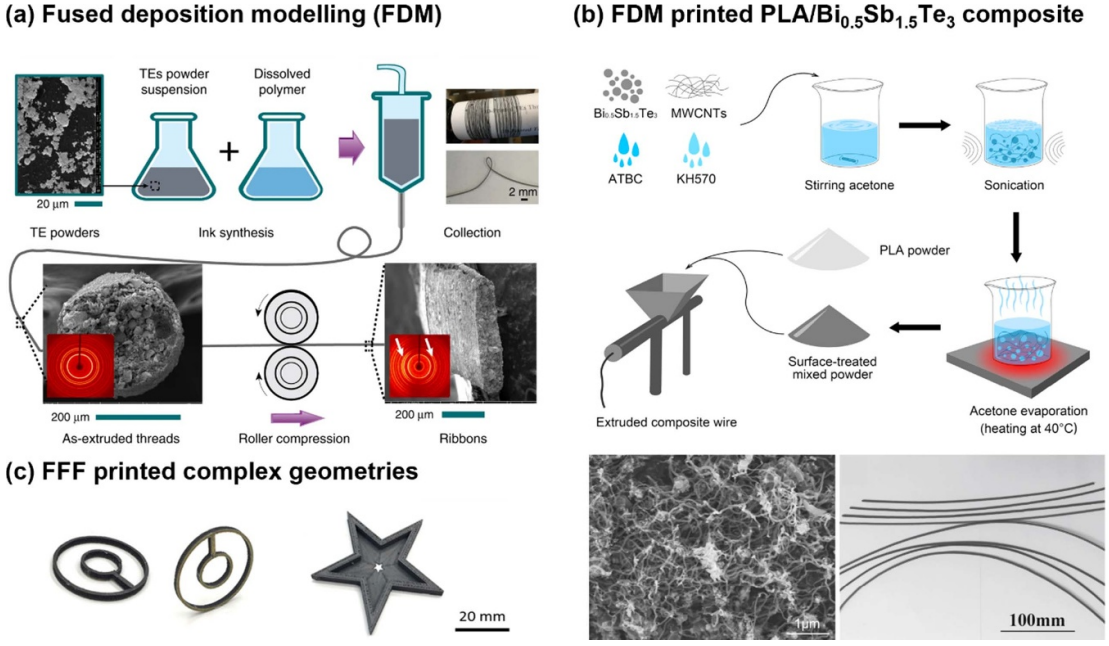

Figure 2. Fused deposition modeling (FDM)-printed TE materials. (a) Schematic diagrams of continuous TE threads production by FDM. Reproduced from [33]. CC BY 4.0. (b) Synthetic processes of BST/PLA composite wires and photograph of extruded BST/PLA composite wires. Reprinted from [65], Copyright (2018), with permission from Elsevier. (c) Schematic representation of FFF fabrication of the TE sample and pictures of the printed TE specimens with various shapes. Reprinted from [67], Copyright (2019), with permission from Elsevier.

showed good flexibility with a bending radius of less than $r_b = 2$ mm, achieved by dispersing TE micrograins within a small amount of a nonconductive polymeric matrixes to create TE composites. In another study, Wang *et al* [65] developed BST/PLA composite TE wires using FDM. They modified the TE and mechanical properties of the wires by varying the loadings of multiwalled carbon nanotubes (MWCNTs), silane coupling agents, and plasticizers (figure 2(b)). For this investigation, PLA, BST powder, and MWCNTs were used as the matrix, filler, and conductive additive, respectively. After the mixing process, they were extruded with a nozzle diameter of 2.5 mm and speeds ranging from 1800 to 2500 mm min^{-1}. The addition of a plasticizer improved the wire flexibility, while increasing the BST content and incorporating MWCNTs considerably enhanced the TE properties. A filament with a $Bi_{0.5}Sb_{1.5}Te_3$/MWCNTs weight ratio of 81.3/4% achieved a maximum ZT value of 0.011 at room temperature. Similarly, Oztan *et al* [67] used organic ABS as a binder to fabricate Bi_2Te_3 via fused filament fabrication (FFF) (figure 2(c)). Composite TE filaments were first extruded from the mixtures and printed into diverse shapes, including concentric cylinders and stars. Heat treatment was performed at 500 °C to decompose the ABS matrix, which considerably improved the TE properties; the resulting ZT of the bulk sample was 0.54 at room temperature Although FDM has many benefits for creating TE materials, it still requires the inclusion of organic polymer binders within the material. Consequently, TE materials produced using FDM often exhibit lower ZT values than those manufactured using dispenser printing or other additive manufacturing methods and to overcome this, there is a significant need for new research, such as the use of organic-free materials and other innovative approaches.

2.3. Powder bed fusion

PBF technology is a subset of additive manufacturing techniques that utilize an energy source to selectively bind or melt powder particles and build object parts layer-by-layer to achieve a desired geometry [68]. The heat sources for PBF can vary and commonly include pulsed lasers and electron beams, especially for metals with high melting points [69]. The categorization of PBF techniques, such as selective laser sintering (SLS), selective laser melting (SLM), direct metal laser sintering, selective heat sintering, and electron beam melting, is based on the energy sources and methods used for material processing [70].

Several studies have explored the fabrication of TE materials using SLM and SLS [34, 71–78]. The SLM technology involves the precise control of a high-energy laser beam for rapidly melting and solidifying powder layers, enabling the creation of bulk materials through the stacking of layers [79]. The key features of this process include rapid cooling rates, which lead to fine-grain structures, and directional grain growth owing to heat loss along the building direction [80]. Taking advantage of these benefits, Qiu *et al* [34]

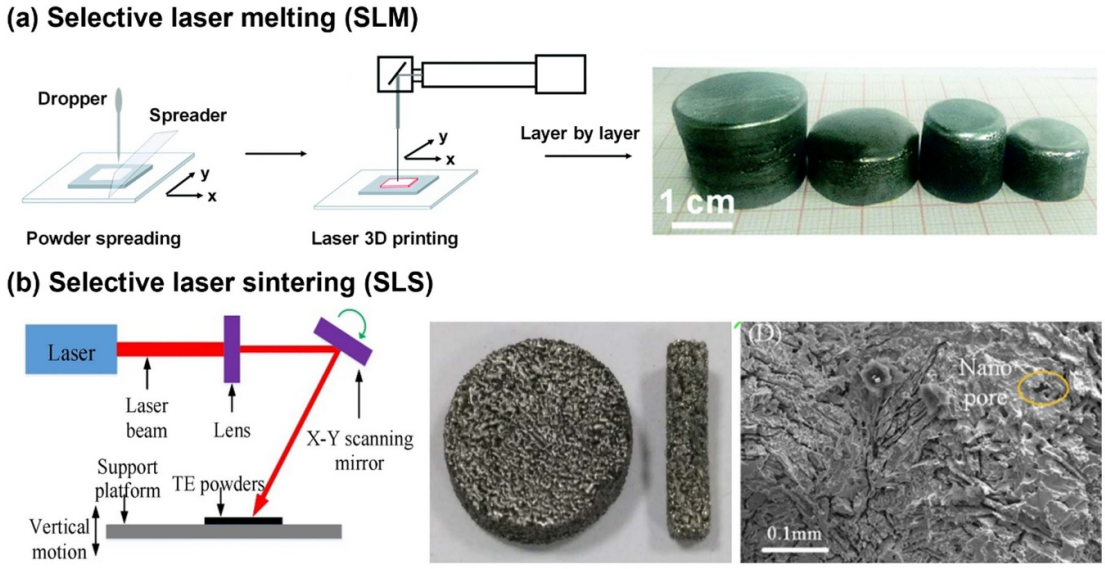

Figure 3. Powder bed fusion (PBF)-printed TE materials. (a) Schematic of the SLM process and photographs of printed samples. Reproduced from [32] with permission from the Royal Society of Chemistry. (b) Schematic of SLS 3D printing setup and image of the printed samples with SEM image showing nano pores. Reprinted from [77], Copyright (2018), with permission from © 2018 The Society of Manufacturing Engineers. Published by Elsevier Ltd. All rights reserved.

developed highly oriented *p*-type BiSbTe polycrystalline bulk materials with remarkable TE performance and outstanding mechanical properties, which were achieved using SLM technology combined with thermal explosions (figure 3(a)). The *p*-type BiSbTe structure printed using a laser with a 100 W power, 1064 nm wavelength, and 100 μm diameter was a strongly oriented polycrystalline material with a very fine grain structure. The orientation factor, near 0.9, closely resembled that of the single crystals produced using zone melting. This directional alignment is a result of the temperature gradient, with heat dissipating along the build direction to minimize the temperature variations between the molten pool and the substrate. In the building direction, the sample achieved a peak *ZT* of 1.1 at 316 K, representing a remarkable 65% increase in comparison to measurements conducted perpendicular to this direction. In addition, the SLM-prepared material exhibited a maximum compressive strength of 91 MPa, surpassing the 80 MPa of the material traditionally prepared using the SPS method. Similarly, Hu *et al* [71] used SLM to fabricate Bi_2Te_3-based TEs with fine-grained structures and nanotwins. Owing to these fine microstructures, the printed TE samples exhibited robust mechanical properties. Moreover, the formation of multiscale defects during the printing process enhanced their TE properties, achieving a maximum *ZT* of 1.27 for the *p*-type and 1.13 for the *n*-type. The SLM technology provides a promising new fabrication route for Bi_2Te_3-based TE materials with a strong grain orientation and an excellent TE performance [34, 71].

SLS starts with a bed of powdered material, and a high-power laser is used to heat and fuse the powdered particles in a cross-sectional pattern. Unlike SLM, SLS utilizes a partial consolidation process, making it more challenging to control the internal microstructure compared to that of SLM [79]. Typically, samples produced using SLS tend to exhibit relatively higher porosity than those created using SLM [79, 81]. For example, Shi *et al* [77] used the SLS method to produce porous $Bi_{0.5}Sb_{1.5}Te_3$ materials with high TE performance. $Bi_{0.5}Sb_{1.5}Te_3$ with a desired porous structure was fabricated by partially melting the powders, focusing on melting only the particle boundaries while preserving the crystalline structures (figure 3(b)). Porosity was controlled by adjusting the energy density of the laser. The optimized processing conditions yielded $Bi_{0.5}Sb_{1.5}Te_3$ structures with numerous micropores while retaining sufficient physical strength. This approach aimed to minimize thermal conductivity while maintaining electrical conductivity. Consequently, the introduction of porosity reduced electrical conductivity by more than 50% compared that of the bulk $Bi_{0.5}Sb_{1.5}Te_3$ alloy. Meanwhile, thermal conductivity experienced a higher decrease of over 75%, resulting a maximum *ZT* of 1.29 at 50 °C. Despite improving TE performance relative to that of conventional TE materials, porous TE structures face limitations owing to their lower mechanical strength [77, 78]. To make them suitable for engineering applications, future research should focus on enhancing both the TE and mechanical properties of porous TE materials fabricated using the SLS method.

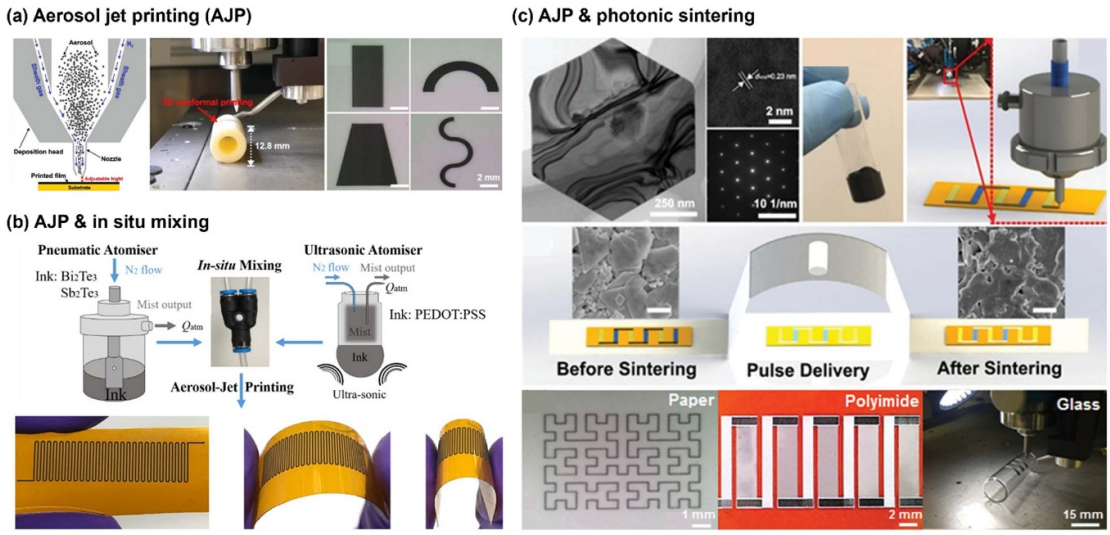

Figure 4. Aerosol-jet-printed TE materials. (a) Schematic of 3D conformal AJP process using solution-processed nanostructures as building blocks and 3D-conformal-printed film on a curved surface to print TE legs with different shapes. Reproduced from [38]. CC BY 4.0. © 2019 The Authors. Published by WILEY-VCH Verlag GmbH & Co. KGaA, Weinheim. (b) Schematic of the novel in situ mixing method for nanocomposite printing by AJP and photographs of the TE nanocomposite printed onto a flexible polyimide sheet, bent to different degrees. Reproduced from [87]. CC BY 4.0. (c) 3D conformal AJP with intense pulsed light sintering of TE films and as-printed films with designed patterns printed on various 2D and 3D substrates. [88] John Wiley & Sons. © 2019 WILEY-VCH Verlag GmbH & Co. KGaA, Weinheim.

2.4. Aerosol jet printing

AJP is an additive manufacturing method that uses a fine aerosol mist to precisely deposit materials onto various substrates [38, 82, 83]. It is versatile and suitable for electronics, sensors, and biomedical devices, with its minimal material waste, light weight, cost-effectiveness [84, 85]. Furthermore, AJP is capable of accommodating inks with a broad spectrum of viscosities and can achieve a resolution of approximately 10 micrometers [86].

Extensive research has been conducted through this process for the production of TE materials [38, 87–89]. Dun *et al* [38] reported high-performance and flexible Sb_2Te_3 films produced by AJP using solution-processable nanostructures as building blocks (figure 4(a)). Sb_2Te_3 nanoplates were fabricated using a hydrothermal method and mixed with ethylene glycol (EG), glycerol, and ethanol at an optimized composition to form a stable ink for AJP. TE films were produced on flat and curved substrates with desired patterns using a colloidal nanocrystal ink, which was followed by thermal sintering to remove surfactants and create a continuous densified network from the initially dispersed nanoparticle assembly. The printed film demonstrated impressive results, including a maximum power factor of 2.2 mW m^{-1} K^{-2} at 500 K, while maintaining its remarkable flexibility, experiencing only a slight 0.6% increase in resistance after enduring 1000 bending cycles with a 7 mm curvature radius. Similarly, Ou *et al* [87] developed a novel insitu mixing method for printing Bi_2Te_3/Sb_2Te_3 and PEDOT:PSS composites by atomizing them separately using AJP (figure 4(b)). PEDOT:PSS and solvothermally synthesized Bi_2Te_3/Sb_2Te_3 nanocrystals were directly printed onto a flexible polyimide sheet and surface-treated with EG to enhance the electrical conductivity. The resulting TE performance of the printed PEDOT:PSS-based nanocomposites was achieved at 85 wt%Sb_2Te_3, with PF of $\sim$28.3μW m K^{-2}. Moreover, the excellent flexibility and mechanical strength of these printed nanocomposites were further validated as the S/S_0 ratio reduced only slightly after extensive flexing at curvatures as high as 300 m^{-1}. Additionally, Saeidi–Javash *et al* [88] developed an 3D conformal AJP method combined with photonic sintering to fabricate high-performance flexible TE devices (figure 4(c)). The group successfully created a printable ink with an appropriate viscosity by blending $Bi_2Te_{2.7}Se_{0.3}$ nanoplates with an optimized solvent. After formulating the ink, it was applied to a flexible 2D substrate to create intricate patterns. These patterns were later subjected to photonic sintering, which effectively removed the organic resin (PVP) and considerably improved the electrical conductivity of the printed film. The electrical conductivity was dramatically enhanced within seconds of photonic sintering, reaching an impressive value of 2.7×10^4 S m^{-1} and exhibiting a power factor of 730 μW m^{-1} K^{-2} at room temperature. AJP, a cost-effective and scalable fabrication process, opens doors for the large-scale production of flexible devices using various high-performance nanoparticle inks.

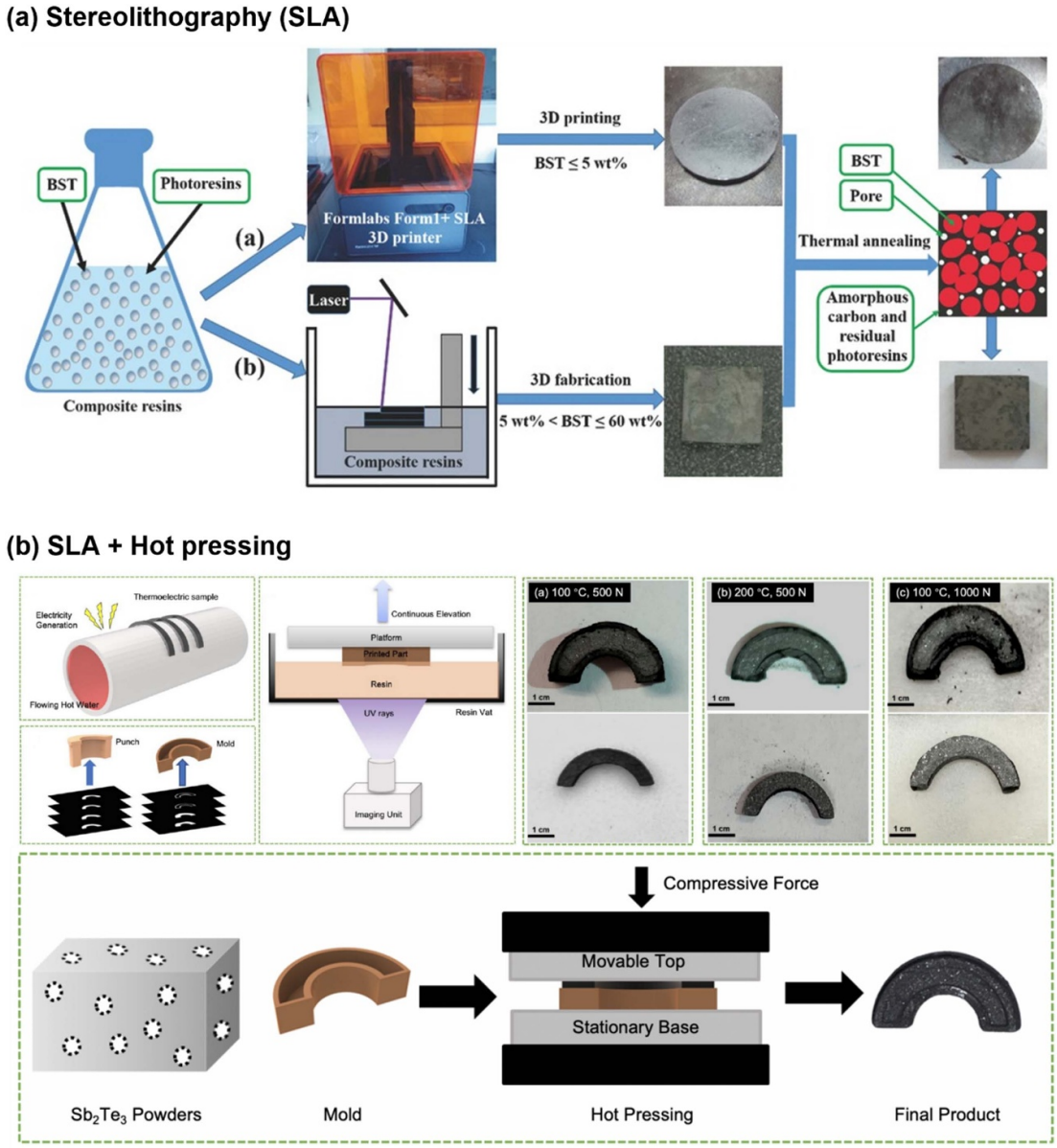

Figure 5. Stereolithography (SLA)-printed TE materials. (a) Schematic routes of 3D printing and 3D fabrication of BST samples mixed with photoresins, followed by thermal annealing. [37] John Wiley & Sons. © 2015 WILEY-VCH Verlag GmbH & Co. KGaA, Weinheim. (b) A schematic illustration of the design process of the mold and relevant punch for TE pipe fabrication using SLA and hot-pressing of Sb_2Te_3 powders with assistance of the SLA-printed mold and punch. Reproduced from [94]. CC BY 4.0.

2.5. Stereolithography

SLA constitutes a 3D printing technique that uses UV light to solidify liquid photopolymer resins in a layer-wise manner, enabling the creation of 3D objects. SLA excels in terms of precision, intricate detailing, and smooth surface finishing, making it versatile for various applications [90, 91]. The printing resolution depends on the dimensions and accuracy of the laser or light source, and the ink must exhibit photopolymerizable properties. This is commonly achieved using photoresins or custom composite inks [92, 93].

To fabricate TE materials through SLA, He *et al* [37] developed printable composite resins by mixing BST powders with photoresin, which enabled them to photocure the composite resins sucessfully with high percentages of BST nanoparticles (figure 5(a)). Using optical equipment, the authors accomplished a layer-by-layer photopolymerization process and conducted thermal annealing to eliminate the residual resin. Although the thermal conductivity was remarkably low at 0.2 W m^{-1} K^{-1}, the low density of the sample resulted in a poor electrical conductivity, yielding a maximum ZT of 0.12 at room temperature. In a recent study, Tiwari *et al* [94] used SLA-printed molds to produce shape-conformal TE materials instead of directly printing TE materials (figure 5(b)). They developed a hybrid approach for manufacturing TE materials through a combination of hot pressing and SLA. Molds and punches were printed using SLA, and Sb_2Te_3

powder was sequentially filled into the SLA-printed mold in a layered manner. The SLA-printed mold was then used to hot-press the Sb_2Te_3 powder into the desired 3D shape. The shape was sintered to fuse the Sb_2Te_3 powder, after which the SLA-printed mold was removed, resulting in the final TE samples. With the integration of hot pressing and SLA, the printed Sb_2Te_3 samples exhibited improved compactness and density, resulting in enhanced electrical properties. Table 2 provides a summary of various printed *p*-type and *n*-type TE materials using different 3D printing methods.

3. Device applications

3.1. Shape conformal TEG

A vital advantage of using 3D printing to manufacture TE materials is its ability to customize the geometry of the TE legs. This customization aids in the producing conformable TE devices that can closely adhere to nonplanar surfaces, such as pipelines. The conformal TE devices exhibit considerably larger temperature gradients within the TE elements owing to the efficient heat transfer that occurs on non-planar surfaces [19]. Consequently, they experience fewer parasitic heat losses than those of nonconformal planar TEGs, resulting in an enhanced TE performance driven by the amplified temperature differences [32]. Figure 6(a) illustrates the fabrication process of the conformal TEG and demonstrates how 3D printing was employed to produce semicircular shapes corresponding to the cylindrical heat source. Several studies have reported the production of such conformal TEGs [32, 42, 52, 55, 71, 95], with a representative example being the work by Kim *et al* [32], who created cylindrical TEGs with dispenser-printed *n*- and *p*-type half-rings using an all-inorganic TE ink (figure 6(b)). The TEG was directly attached onto an alumina tube, which achieved a maximum output voltage of 27.0 mV and a maximum power of 1.62 mW at $\Delta T = 39$ K. The output power density was 1.42 mW cm^{-2} at the same temperature difference. To validate the effectiveness of shape-conformable TE devices, the authors constructed a 3D finite element model (FEM) and conducted a computational comparison of the power generation (figure 6(f)). This involved comparing the conformal TEG against a conventional planar TEG constructed on an alumina pipe under identical environmental conditions. The temperature gradient within the TE components (ΔT_{TE}) was approximately 2 times greater in the half ring-based TEG compared to that of the planar TEGs due to its effective thermal contacts with curved heat sources. Consequently, for the half ring-based TEG, both η_{TE} and η_{system} were found to be 1.2–3.6 and 1.1–4.7 times greater than those of the planar TEG, respectively. Similarly, Su *et al* [52] manufactured annular devices through dispenser printing using a TE ink containing an organic binder, resulting in an output voltage of 60.8 mV and a maximum output power of 0.68 mW at $\Delta T_{TE} = 54.6$ K. This result is consistent with the FEM simulation results (figure 6(c)). Subsequently, Wang *et al* [95] also produced half-angular legs with a quasi-inorganic TE ink using dispenser printing, and the devices achieved an output voltage of 40.61 mV and a power output of 0.38 mW at $\Delta T_{TE} = 55$ K (figure 6(d)). In addition to dispenser printing, Hu *et al* [71] manufactured shape-conformal TEGs using SLM technology (figure 6(e)). They designed a well-shape-controllable and high-performance TEG using SLM-printed Bi_2Te_3 half-rings, achieving an output power of 134 mW at $\Delta T_{TE} = 38.9$ K. Therefore, 3D printing technology creates opportunities for crafting shape-conformable and well-designed TE modules, thereby fostering the expectation of improved efficiency and power density in various TEG applications.

3.2. Flexible TEG

TE power generators, which convert body heat into electrical energy, offer valuable prospects for powering self-sustaining wearable mobile electronic systems [98–100]. To produce wearable self-powered electronic devices, there has been growing demand for flexible TE devices capable of maintaining robust mechanical stability under repeated mechanical stress [101]. As previously mentioned, an advantage of 3D printing technology is its ability to print on various substrates and control the thickness of the printed TE materials. This process allows for the efficient and straightforward production of flexible TE modules. Recently, numerous studies have focused on developing wearable and flexible TE generators through 3D printing [33, 58, 88]. For example, Chen *et al* [58] reported a planar prototype device consisting of 50 pairs. The device was manufactured through dispenser printing on a flexible polyimide substrate (figure 7(a)). Metal contacts were deposited via shadow mask evaporation while TE elements were dispenser-printed onto a flexible polyimide substrate with a thickness of 50.8 μm. The device was then completed by rolling the substrate into a coil and securing it with polyimide tape, resulting in an output of 10.5 μW at $\Delta T_{TE} = 20$ K. Peng *et al* [33] developed a wearable TE device composed of flexible TE threads manufactured using FDM (figure 7(b)). The flexibility of the threads was attained by dispersing the TE micrograins within the nonconductive polymeric matrix. Remarkably, the resistance and seebeck coefficient of the threads remained unchanged after hundreds of bending cycles with a radius of 6 mm during bending tests. Flexible TE modules were then fabricated by interleaving *p*-type and *n*-type threads on Kapton substrates, which achieved optimal power

Table 2. TE properties and power performance of 3D printed TE materials.

TE materials	Additive	Viscosity (Pa·s)	Process	Electrical conductivity (S cm $^{-1}$)	Seebeck coefficient (μV K^{-1})	Thermal conductivity (W m^{-1} K^{-1})	ZT	Output power	References
Bi_2Te_3	PLGA	40	Dispenser printing	≈ 750	≈ -100	≈ 1.27	0.33	N/A	[53]
$Bi_{0.5}Sb_{1.5}Te_3$ Bi_2Te_3	PVP	10^3	Dispenser printing	76.2	152.7	0.543	0.104	0.68 mW ($\Delta T = 55$ K)	[52]
				103.3	-135	0.573	0.11		
Bi_2Te_3	Se/Epoxy	N/A	Dispenser printing	96	-170	0.38	0.31	25 μW ($\Delta T = 20$ K)	[96]
Bi_2Te_3	Se/Epoxy	N/A	Dispenser printing	20	200	0.27	0.17	1.6 μW ($\Delta T = 20$ K)	[57]
Sb_2Te_3 Bi_2Te_3	Epoxy	N/A	Dispenser printing	40	170	0.24	0.19	10.5 μW ($\Delta T = 20$ K)	[58]
				30	-160	0.24	0.18		
$Bi_{0.5}Sb_{1.5}Te_3$ Bi_2Te_3	Epoxy	N/A	Dispenser printing	14.4	272	0.52	0.061	N/A	[59]
				8	-159	0.48	0.0126		
$Bi_{0.4}Sb_{1.6}Te_3$ $Bi_2Te_{2.6}Se_{0.4}$	PVP	N/A	Dispenser printing	280	212	0.72	0.56	N/A	[97]
				330	-160	0.89	0.68		
$Bi_{0.5}Sb_{1.5}Te_3$	Pluronic F127	≈ 1300 at 1 s^{-1}	Dispenser printing	≈ 10	≈ 170	≈ 0.09	0.187	N/A	[55]
$Bi_{0.5}Sb_{1.5}Te_3$ $Bi_{2.0}Te_{2.7}Se_{0.3}$	PAA, PEI	4×10^4	Dispenser printing	≈ 780	≈ 143	≈ 0.98	≈ 0.71	0.38 mW ($\Delta T = 56$ K)	[95]
				≈ 515	≈ -148	≈ 0.81	$\approx$0.59		
$Bi_{0.5}Sb_{1.5}Te_3$ $Bi_2Te_{2.7}Se_{0.3}$	ChaM (Sb_2Te_3)	8.3×10^2	Dispenser printing	554	165	0.63	0.9	1.62 mW ($\Delta T = 39$ K)	[32]
				500	120	0.57	0.68		
$Bi_{0.55}Sb_{1.45}Te_3$	ChaM ($Sb_2Te_4^{2-}$)	10^5	Dispenser printing	623	200	0.77	1.05	259 mW ($\Delta T = 236$ K)	[54]
$Bi_{0.55}Sb_{1.45}Te_3$ $Bi_2Te_{2.7}Se_{0.3}$	ChaM ($Sb_2Te_4^{2-}$)	8×10^4	Dispenser printing	677	197	0.856	0.9	2.8 μW ($\Delta T = 83$ K)	[48]
				818	-110	0.8	0.68		
Bi_2Te_3	ABS	N/A	FDM	≈ 54	≈ 240	≈ 0.17	0.54	N/A	[67]
$Bi_{0.5}Sb_{1.5}Te_3$	MWCNTs/PLA	N/A	FDM	3.54	178.7	0.31	0.011	N/A	[65]
$Bi_{0.5}Sb_{1.5}Te_3$ $Bi_2Te_{2.7}Se_{0.3}$	PLG	N/A	FDM	6	240	0.25	0.08	26.2 nW ($\Delta T = 10$ K)	[33]
				1	-120	0.25	0.005		
$Bi_{0.4}Sb_{1.6}Te_3$	PLA	N/A	FDM	13.1	125.5	0.28	0.024	N/A	[66]

(Continued.)

Table 2. (Continued.)

$Bi_{0.4}Sb_{1.6}Te_3$/Ag	PLA	N/A	FDM	1170	80	N/A	N/A	N/A	[64]
$Bi_2Te_{2.7}Se_{0.3}$	Tween 20	0.35	Dispenser printing + SLM	$\approx$ 1220	105	2.2	0.3	N/A	[76]
$Bi_{0.5}Sb_{1.5}Te_3$ $Bi_{0.5}Te_{2.7}Se_{0.3}$	N/A	N/A	SLM	$\approx$ 1150	$\approx$ 195	$\approx$ 1.11	1.27	134 mW ($\Delta T = 39$ K)	[71]
				$\approx$ 900	≈ -155	$\approx$ 1.01	1.13		
$Bi_{0.4}Sb_{1.6}Te_3$	N/A	N/A	SLM	1180	192	1.1	1.1	1.42 W ($\Delta T = 120$ K)	[34]
$Bi_2Te_{2.7}Se_3$	N/A	N/A	SLM	830	-156	1.7	0.84	N/A	[72]
Sb_2Te_3	N/A	N/A	SLM	3520	73	$\approx$ 2.9	0.4	N/A	[73]
Bi_2Te_3	N/A	N/A	SLM	N/A	N/A	N/A	N/A	N/A	[74]
Bi_2Te_3	N/A	N/A	SLM	$\approx$ 103	-165	$\approx$ 0.85	0.11	N/A	[75]
$Bi_{0.5}Sb_{1.5}Te_3$	N/A	N/A	SLM	$\approx$ 340	$\approx$168	0.27	1.29	N/A	[77]
$Bi_2Te_{2.85}Se_{0.15}$	Epoxy	N/A	SLS	$\approx$ 345	≈ -145	$\approx$ 0.29	0.88	N/A	[78]
$Bi_{0.5}Sb_{1.5}Te_3$	Photoresin	N/A	SLA	48	147	0.25	0.12	N/A	[37]
Sb_2Te_3	N/A	N/A	SLA + HP	N/A	N/A	N/A	N/A	N/A	[94]
Bi_2Te_3/Sb_2Te_3 /PEDOT:PSS	N/A	N/A	Aerosol jet printing	$\approx$ 247	$\approx$ 34	N/A	N/A	N/A	[87]
$Bi_2Te_{2.7}Se_{0.3}$	PVP	N/A	Aerosol jet printing	$\approx$ 270	≈ -150	N/A	N/A	141 nW ($\Delta T = 50$ K)	[88]
Bi_2Te_3	PVP	N/A	Aerosol jet printing	$\approx$ 250	≈ -110	N/A	N/A	N/A	[89]
Sb_2Te_3	N/A	N/A	Aerosol jet printing	$\approx$ 628	147	N/A	N/A	1.15 nW ($\Delta T = 60$ K)	[38]

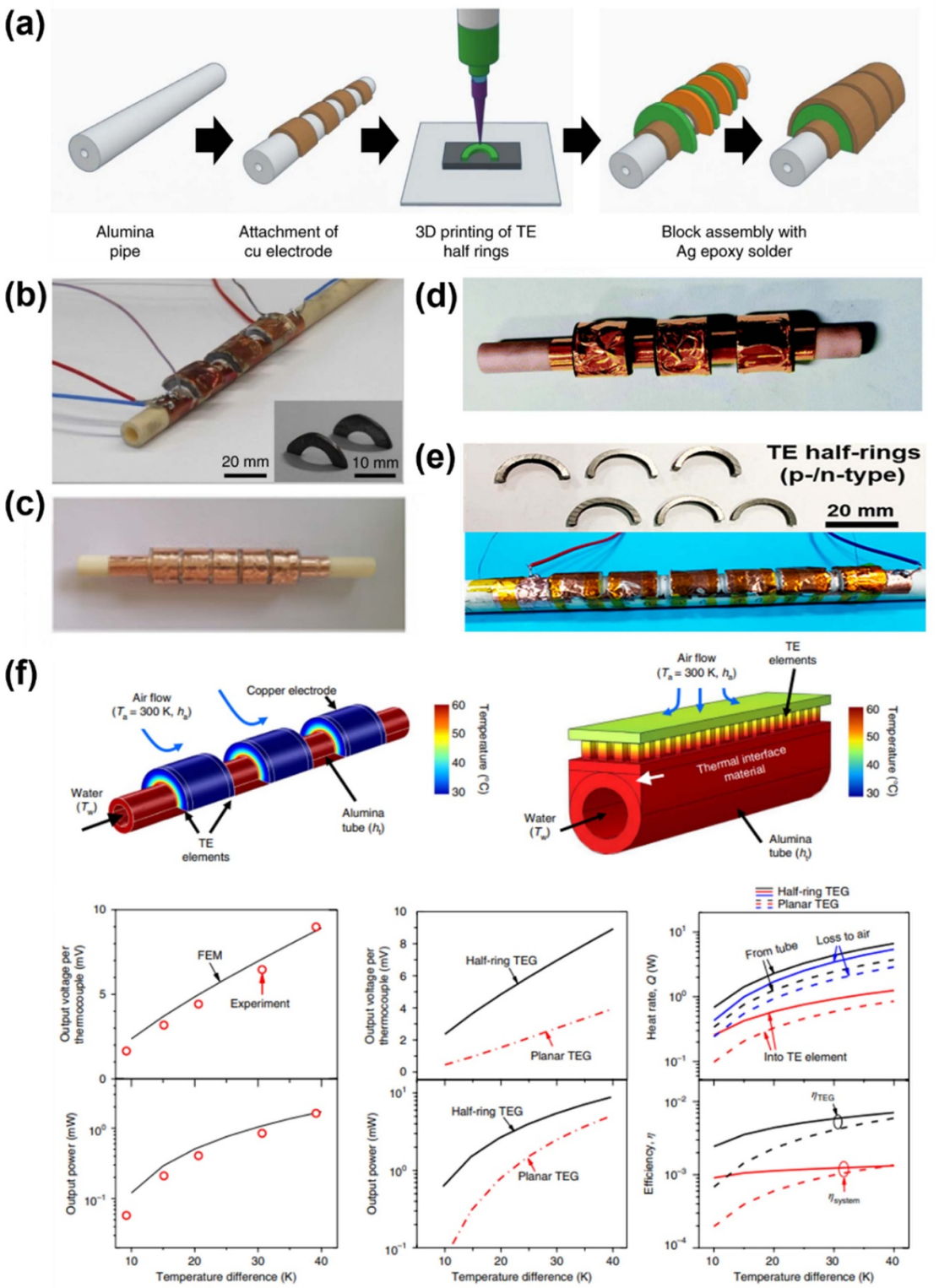

Figure 6. Shape conformal TEG fabricated via 3D printing. (a) A scheme showing the fabrication of the shape conformal TEG using dispenser printing. (b) Photographs of the half-ring-based conformal TEG. The inset shows the dispenser printed *n*-type and *p*-type half rings. (a) and (b) Reproduced from [32], with permission from Springer Nature. (c) Photograph of the annular device containing five pairs of TE legs. Reprinted from [52], Copyright (2020), with permission from Elsevier. (d) Photograph of the half-annular TE module. Reproduced from [95] with permission from the Royal Society of Chemistry. (e) Photographs of SLM-printed half-rings and fabricated half-ring TEGs. Photograph of the half-annular TE module. Reprinted with permission from [71]. Copyright (2023) American Chemical Society. (f) Comparative simulation study of the conformal and planar TEGs on an alumina pipe. Reproduced from [32], with permission from Springer Nature.

outputs of 26.2 nW (in parallel) and 3.4 nW (in a vertical orientation) for five threads. Similarly, Saeidi–Javash *et al* [88] studied the development of flexible devices utilizing $Bi_2Te_{2.7}Se_{0.3}$ nanoplate inks, which were suitable for printing on nearly any flexible substrate using AJP (figure 7(c)). The precise control

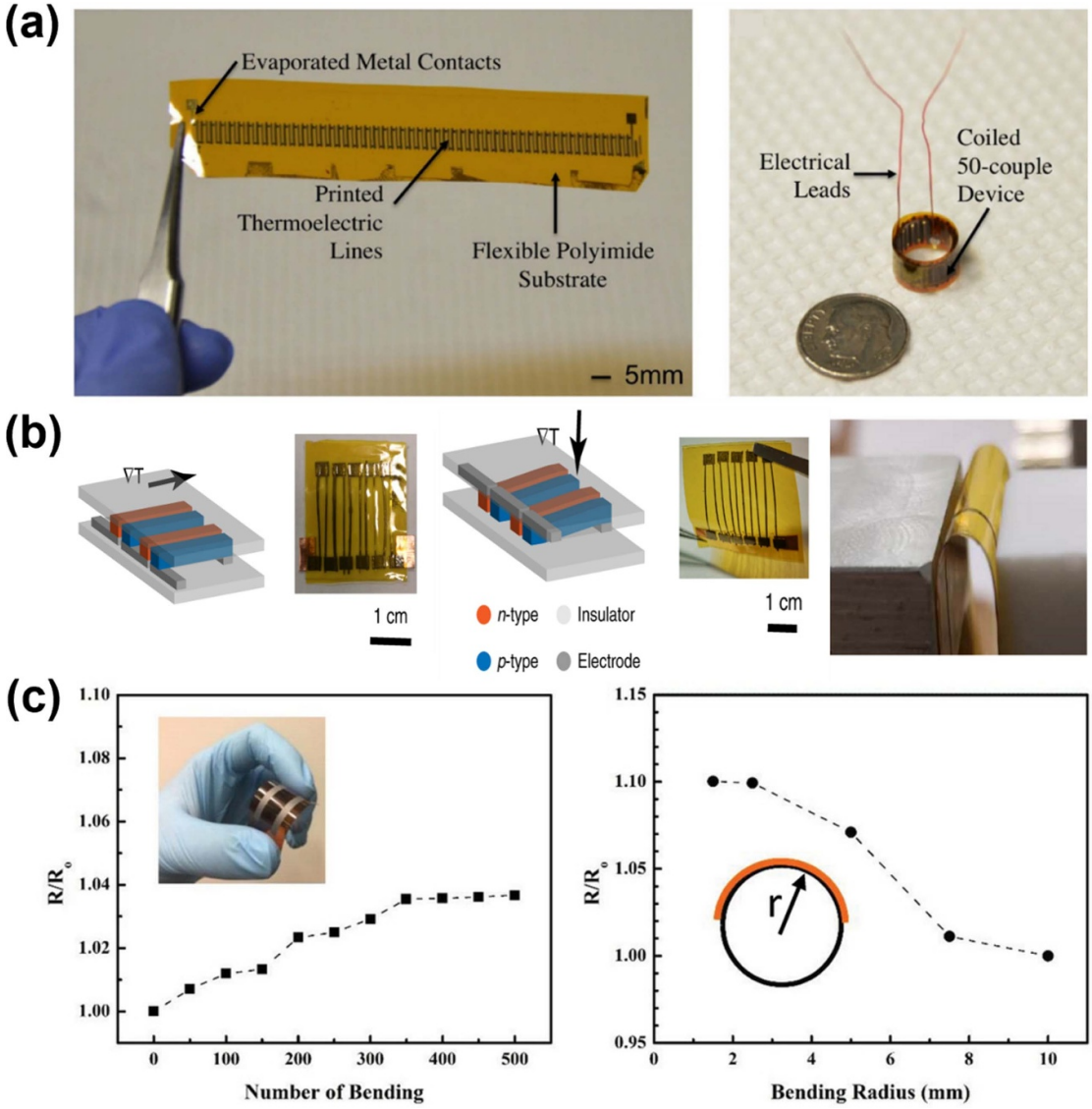

Figure 7. Wearable/flexible TEG fabricated via 3D printing. (a) Images of dispenser-printed 50-couple planar TE device on a flexible polyimide substrate and coiled prototype with electrical connections. Reproduced from [58]. © IOP Publishing Ltd. All rights reserved. (b) Schematics and pictures indicating FDM-fabricated TE modules with thermal gradient parallel and transverse to the thread direction. The right picture indicates a bending radius $r_b = 5$ mm of a *p*-type thread held over a flexible Kapton plastic support. Reproduced from [33]. CC BY 4.0. (c) Mechanical properties of aerosol jet-printed $Bi_2Te_{2.7}Se_{0.3}$ thin films on polyimide. [88] John Wiley & Sons. © 2019 WILEY-VCH Verlag GmbH & Co. KGaA, Weinheim.

of the thickness during the printing process endowed the resulting TE devices with remarkable mechanical flexibility and stability. Only a minor change (4%) in the film resistance was recorded after 500 bending cycles. The flexible TEG featuring aerosol jet-printed $Bi_2Te_{2.7}Se_{0.3}$ films achieved a maximum power output of 141 nW and a power density of 2.7 mW cm^{-2} at $\Delta T_{TE} = 50$ K. These studies confirmed the effectiveness of the flexible TE generator in generating electricity from body heat and providing power autonomy to portable micro-watt electronic devices.

3.3. Micro TE module (thermal management)

Micro TE modules (μTEMs) can generate power from minimal heat flow or act as coolers for localized heat management, making them suitable for integration into various emerging systems, including the Internet of things, wearable devices, wireless sensor networks, and lab-on-a-chip devices [102, 103]. The adoption of 3D printing technology with microlevel precision offers a straightforward, swift, and cost-efficient manufacturing solution for producing micro-TE modules. Recently, the DIW process of Bi_2Te_3 TE materials was used to fabricate μTEGs (figure 8(a)) [48]. The shape engineerability of the process made it possible to design TE legs for optimized thermal transfer, maximizing the temperature gradient and the resulting output power of μTEGs. TE filaments with a diameter of 350 μm and a height of 1400 μm were successfully fabricated via DIW. The μTEG, constructed using these TE filaments, achieved a maximum output voltage of

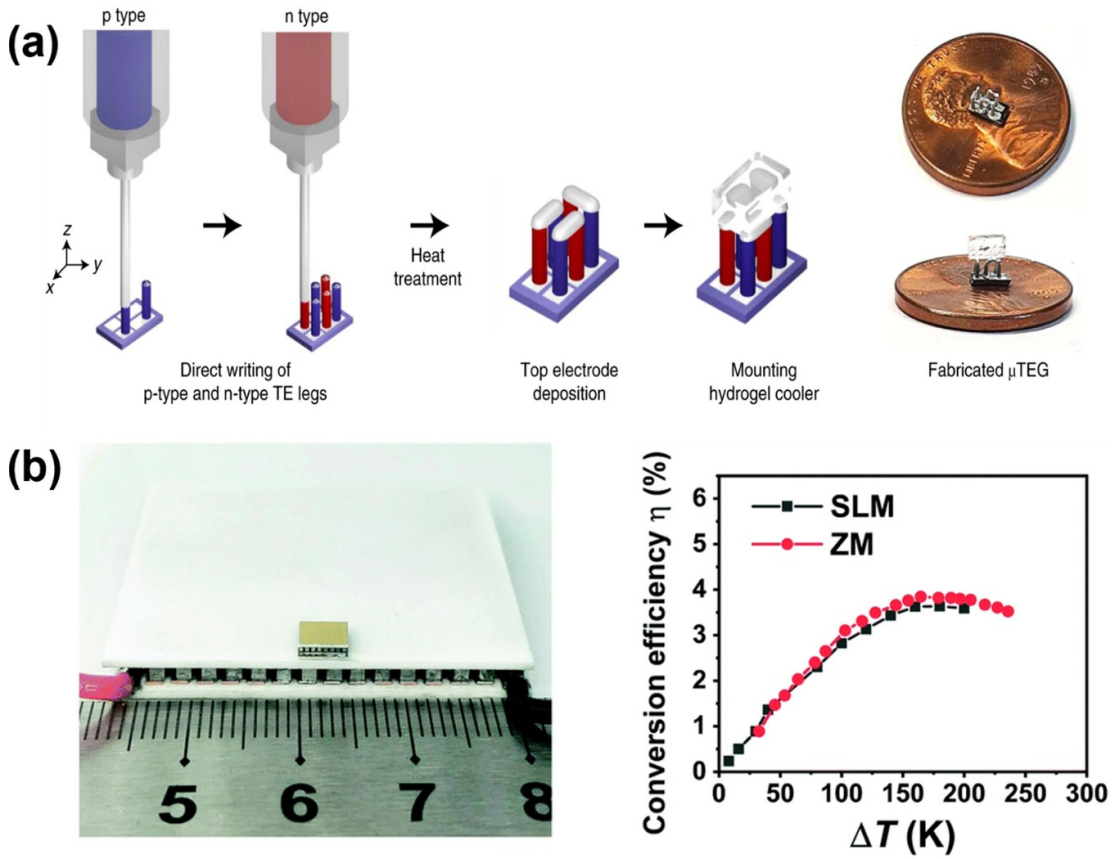

Figure 8. Micro TE devices fabricated via 3D printing. (a) Schematic showing the fabrication of the μTEG by direct 3D ink writing. Reproduced from [48], with permission from Springer Nature. (b) A photograph of SLM-fabricated micro-TE modules and comparison of the conversion efficiencies of the conventional modules made from zone melting and SLM materials. Reproduced from [34] with permission from the Royal Society of Chemistry.

42.4 mV and produced 2.8 μW of power at $\Delta T_{TE} = 82.9$ K. Similarly, Qiu *et al* [34] manufactured μTEMs based on $Bi_{0.4}Sb_{1.6}Te_3$ with a strong preferential orientation using SLM (figure 8(b)). They fabricated a micro module with dimensions of 4 mm × 4 mm × 1.2 mm, and the size and number of leg pairs were 0.36 mm × 0.36 mm × 0.53 mm and 28, respectively. The conversion efficiencies of the macromodules made of both zone melting and SLM *p*-type materials were the same, with the maximum conversion efficiency reaching close to 4% at $\Delta T_{TE} = 170$ K. However, the cooling performance of the SLM-printed micro-TE module, with a maximum cooling temperature difference of 61.78 K, was better than that of the SPS-based micro-module. Owing to the simplicity of the process and excellent device performance, 3D printing technology offers a promising new fabrication method for Bi_2Te_3-based micro-TE devices.

4. Conclusion and perspectives

This article reviews recent progress in the 3D printing fabrication of TE materials and devices, mainly focusing on various printing methods and device applications. It shows that 3D printing technology offers numerous advantages over conventional device fabrication methods. First, 3D printing considerably improves manufacturability by simplifying the intricate and time-consuming processes of traditional manufacturing. The streamlined 3D printing process and meticulous control over material utilization significantly enhance both production efficiency and cost-effectiveness. Another key advantage is its geometrical flexibility, which enables the creation of complex and customized geometries that were previously challenging or unattainable. This flexibility allows for the optimization of the shape and structures of system, including the design of a heat sink, modulation of interfacial thermal resistances, and optimization of design parameters for TE legs. The thermal design strategy for TE devices is focused on producing a significant temperature difference, thereby contributing to the improvement in device power performance. Moreover, the versatility of 3D printing enables the utilization of a wide range of materials, including both organic and inorganic materials, as well as hybrid composite materials.

Although 3D printing of TE materials and modules has been established as a new fabrication route in the TE community, many unresolved challenges remain to be investigated within academia. To achieve an enhanced efficiency in systems with printed TE materials, researchers should thoroughly seek a comprehensive understanding and systematic optimization of 3D printing inks and 3D-printed TE materials, 3D module design and fabrication, and system-level applications. In the context of implementing 3D printing technology for TE material production, it is crucial to transform TE materials into a printable format to satisfy the requirements of diverse 3D printing methods. This transformation can be achieved by integrating organic binders and additives. However, these supplementary components have a high negative impact on the material efficiency, which is why most 3D-printed TE materials developed thus far exhibit notably low ZT values. Although all-inorganic printable materials with excellent TE properties have been developed recently [32, 48, 54], the exploration of well-established approaches for achieving ZT values remains limited, including doping, composition optimization, microstructure engineering, and nanostructuring [7–18]. Moreover, printed TE materials frequently exhibit inferior mechanical properties, which can be attributed to the inherent porosity that occurred during printing or the vaporization of organic binders. In addition, the layer-by-layer production process often results in anisotropic mechanical properties, with the interface between adjacent layers experiencing the highest residual stresses [34]. To enable their use in diverse harvesting applications, researchers must prioritize the production of denser TE materials through the optimization of the printing and sintering processes.

The 3D printing of TE materials in the current status may not show the advantage for traditional planar-structured TE modules. In TE module design, the research has mainly focused on reducing the thermal interface resistance with shape conformability or basic geometric optimization of TE legs [32, 43]. This stands in stark contrast to the well-established field of 3D printing in mechanics, where a wide range of design tools has been extensively combined with 3D printing over many years, offering a new way to improve the mechanical properties of materials by geometrical control. However, the 3D printing technology for TE materials and devices is still in its development phase and further advancements combined with 3D thermal design would enable to adapt them to diverse thermal environments and ultimately contribute to enhancing the intrinsic efficiency. For example, a recent study demonstrates that TE legs with cellular structures can exhibit higher energy conversion efficiency than that of a typical cuboid by improving the thermal spreading efficiency [43]. However, a sophisticated and detailed geometric design is crucial for improving the system-level efficiency, necessitating innovative approaches using software tools. To achieve this, it is necessary to build a cohesive collaborative network that connects the diverse realms of TE research and geometric design. Although in-depth exploration of TE design for improving TE efficiency has not been extensively explored to date, we believe that the combination of 3D printing with thermal design tools will emerge as another means to enhance TE efficiency in the near future.

In the context of mass production, the 3D printing process can be beneficial to reduce the production cost of TE modules since it enables maximizing the usage of raw elements. Generally, ∼60% of raw material is lost in the manufacturing process of TE modules due to the composition inhomogeneity in the synthesized ingot and the loss during the dicing process. Additionally, the 3D printing process could also simplify the overall manufacturing process by eliminating the need for dicing and leg positioning processes. However, further efforts are necessary to achieve practical applications and industrialization of 3D-printed TE materials. First, the durability of printed TE materials is still substantially lower than that of bulk TE ingots because of their porous structures and degradation of the thermal and electrical interfaces with thermal expansion mismatch. To realize printed TE devices with a competitive mechanical stability, various approaches need to be explored, including novel post-printing processes that reduce the porosity of TE materials and optimization of design of TE leg to minimize interface mismatches and thermal expansion discrepancies. Second, most studies on 3D-printed TE devices have not paid much attention to elemental technologies involving electrode materials, bonding techniques, and diffusion barriers in systems engineering, despite their importance in the practical implementation of TE devices. The power performance of TE devices is inversely proportional to the device resistance. It is imperative to acknowledge that device resistance encompasses not only the inherent resistance of TE materials but also the indispensable inclusion of contact resistance, often manifesting as the dominant factor. For example, silver (Ag)-based inks or pastes are primarily used as solders or electrode materials in applications such as shape-conformal TEGs. However, these Ag pastes exhibit lower adhesive strengths and higher contact resistances than traditional bulk solder bonding materials. Recent advancements in conductive inks and pastes, such as graphene and silver nanoparticles [104, 105], offer the potential to achieve a low contact resistance with inorganic materials, enabling an all-printing process for TEGs. In addition, the diffusion barrier between TE materials and electrodes should be studied for the durability of the printed TE devices at high temperatures. Finally, to efficiently harness substantial waste heat in large-scale applications, such as ships and factories, it is crucial to fabricate large-scale TE devices and mass commercialization. To achieve this, it is essential to manufacture

TE materials with uniform TE properties over a large area and to establish an optimized production process that is both time- and cost-efficient. Advancements in these technologies can encourage the research of 3D printed TE devices as renewable energy sources to enhance electricity supply.

Data availability statement

The data that support the findings of this study are available upon reasonable request from the authors.

Acknowledgments

This work was supported by the National Research Foundation of Korea (NRF) grant funded by the Korea government (MSIT) (NRF-2022R1A2C3009129; NRF-2022M3H4A1A04076667).

ORCID iD

J S Son https://orcid.org/0000-0003-3498-9761

References

[1] Brockway P E, Owen A, Brand-Correa L I and Hardt L 2019 Estimation of global final-stage energy-return-on-investment for fossil fuels with comparison to renewable energy sources *Nat. Energy* **4** 612–21
[2] Barnes P W *et al* 2019 Ozone depletion, ultraviolet radiation, climate change and prospects for a sustainable future *Nat. Sustain.* **2** 569–79
[3] Hochbaum A I, Chen R, Delgado R D, Liang W, Garnett E C, Najarian M, Majumdar A and Yang P 2007 Enhanced thermoelectric performance of rough silicon nanowires *Nature* **451** 163–7
[4] Zebarjadi M, Esfarjani K, Dresselhaus M S, Ren Z F and Chen G 2012 Perspectives on thermoelectrics: from fundamentals to device applications *Energy Environ. Sci.* **5** 5147
[5] Snyder G J and Toberer E S 2008 Complex thermoelectric materials *Nat. Mater.* **7** 105–14
[6] Wood C 1988 Materials for thermoelectric energy-conversion *Rep. Prog. Phys.* **51** 459–539
[7] Kim S I *et al* 2015 Dense dislocation arrays embedded ingrain boundaries for high-performancebulk thermoelectrics *Science* **348** 109–14
[8] Zhao L-D, Lo S-H, Zhang Y, Sun H, Tan G, Uher C, Wolverton C, Dravid V P and Kanatzidis M G 2014 Ultralow thermal conductivity and high thermoelectric figure of merit in SnSe crystals *Nature* **508** 373–7
[9] Qiu P *et al* 2019 High-efficiency and stable thermoelectric module based on liquid-like materials *Joule* **3** 1538–48
[10] Duong A T *et al* 2016 Achieving ZT=2.2 with Bi-doped n-type SnSe single crystals *Nat. Commun.* **7** 13713
[11] Jo S *et al* 2016 Simultaneous improvement in electrical and thermal properties of interface-engineered BiSbTe nanostructured thermoelectric materials *J. Alloys Compd.* **689** 899
[12] Son J S *et al* 2012 n-type nanostructured thermoelectric materials prepared from chemically synthesized ultrathin Bi_2Te_3 nanoplates *Nano Lett.* **12** 640–7
[13] Wei W *et al* 2018 Achieving high thermoelectric figure of merit in polycrystalline SnSe via introducing Sn vacancies *J. Am. Chem. Soc.* **140** 499
[14] Poudel B *et al* 2008 High-thermoelectric performance of nanostructured bismuth antimony telluride bulk alloys *Science* **320** 634–8
[15] Son J S, Zhang H, Jang J, Poudel B, Waring A, Nally L and Talapin D V 2014 All-inorganic nanocrystals as a glue for BiSbTe grains: design of interfaces in mesostructured thermoelectric materials *Angew. Chem., Int. Ed.* **53** 7466–70
[16] Heremans J P, Jovovic V, Toberer E S, Saramat A, Kurosaki K, Charoenphakdee A, Yamanaka S and Snyder G J 2008 Enhancement of thermoelectric efficiency in PbTe by distortion of the electronic density of states *Science* **321** 554–7
[17] Heo S H *et al* 2019 Composition change-driven texturing and doping in solution-processed SnSe thermoelectric thin films *Nat. Commun.* **10** 846
[18] Jiang B *et al* 2021 High-entropy-stabilized chalcogenides with high thermoelectric performance *Science* **371** 830–4
[19] Shittu S, Li G, Zhao X and Ma X 2020 Review of thermoelectric geometry and structure optimization for performance enhancement *Appl. Energy* **268** 115075
[20] Wang C-C, Hung C-I and Chen W-H 2012 Design of heat sink for improving the performance of thermoelectric generator using two-stage optimization *Energy* **39** 236–45
[21] LeBlanc S 2014 Thermoelectric generators: linking material properties and systems engineering for waste heat recovery applications *Sustain. Mater. Technol.* **1–2** 26–35
[22] He Z-Z 2020 A coupled electrical-thermal impedance matching model for design optimization of thermoelectric generator *Appl. Energy* **269** 115037
[23] Thimont Y and LeBlanc S 2019 The impact of thermoelectric leg geometries on thermal resistance and power output *J. Appl. Phys.* **126** 095101
[24] Xing Y *et al* 2019 High-efficiency half-Heusler thermoelectric modules enabled by self-propagating synthesis and topologic structure optimization *Energy Environ. Sci.* **12** 3390–9
[25] Zhuang H-L, Pei J, Cai B, Dong J, Hu H, Sun F-H, Pan Y, Snyder G J and Li J-F 2021 Thermoelectric performance enhancement in BiSbTe alloy by microstructure modulation via cyclic spark plasma sintering with liquid phase *Adv. Funct. Mater.* **31** 2009681
[26] Muthiah S, Singh R C, Pathak B D, Avasthi P K, Kumar R, Kumar A, Srivastava A K and Dhar A 2018 Significant enhancement in thermoelectric performance of nanostructured higher manganese silicides synthesized employing a melt spinning technique *Nanoscale* **10** 1970–7
[27] Xie W, Tang X, Yan Y, Zhang Q and Tritt T M 2009 Unique nanostructures and enhanced thermoelectric performance of melt-spun BiSbTe alloys *Appl. Phys. Lett.* **94** 102111

[28] Xu Z J, Hu L P, Ying P J, Zhao X B and Zhu T J 2015 Enhanced thermoelectric and mechanical properties of zone melted p-type $(Bi,Sb)_2Te_3$ thermoelectric materials by hot deformation *Acta Mater.* **84** 385–92
[29] Pan Y, Wei T-R, Cao Q and Li J-F 2015 Mechanically enhanced p- and n-type Bi_2Te_3-based thermoelectric materials reprocessed from commercial ingots by ball milling and spark plasma sintering *Mater. Sci. Eng.* B **197** 75–81
[30] Zhang Q, Liao J, Tang Y, Gu M, Ming C, Qiu P, Bai S, Shi X, Uher C and Chen L 2017 Realizing a thermoelectric conversion efficiency of 12% in bismuth telluride/skutterudite segmented modules through full-parameter optimization and energy-loss minimized integration *Energy Environ. Sci.* **10** 956–63
[31] LeBlanc S, Yee S K, Scullin M L, Dames C and Goodson K E 2014 Material and manufacturing cost considerations for thermoelectrics *Renew. Sustain. Energy Rev.* **32** 313
[32] Kim F *et al* 2018 3D printing of shape-conformable thermoelectric materials using all-inorganic Bi_2Te_3-based inks *Nat. Energy* **3** 301–9
[33] Peng J *et al* 2019 3D extruded composite thermoelectric threads for flexible energy harvesting *Nat. Commun.* **10** 5590
[34] Qiu J *et al* 2019 3D Printing of highly textured bulk thermoelectric materials: mechanically robust BiSbTe alloys with superior performance *Energy Environ. Sci.* **12** 3106–17
[35] Park S H *et al* 2016 High-performance shape-engineerable thermoelectric painting *Nat. Commun.* **7** 13403
[36] Jo S, Choo S, Kim F, Heo S H and Son J S 2018 Ink processing for thermoelectric materials and power-generating devices *Adv. Mater.* **31** 1804930
[37] He M, Zhao Y, Wang B, Xi Q, Zhou J and Liang Z 2015 3D printing fabrication of amorphous thermoelectric materials with ultralow thermal conductivity *Small* **11** 5889–94
[38] Dun C, Kuang W, Kempf N, Saeidi-Javash M, Singh D J and Zhang Y 2019 3D printing of solution-processable 2D nanoplates and 1D nanorods for flexible thermoelectrics with ultrahigh power factor at low-medium temperatures *Adv. Sci.* **6** 1901788
[39] Lewis J A and Ahn B Y 2015 Device fabrication: three-dimensional printed electronics *Nature* **518** 42–43
[40] Ngo T D, Kashani A, Imbalzano G, Nguyen K T Q and Hui D 2018 Additive manufacturing (3D printing): a review of materials, methods, applications and challenges *Composites* B **143** 172–96
[41] Wilkinson N J, Smith M A A, Kay R W and Harris R A 2019 A review of aerosol jet printing—a non-traditional hybrid process for micro-manufacturing *Int. J. Adv. Manuf. Technol.* **105** 4599–619
[42] Lee J *et al* 2021 Doping-induced viscoelasticity in PbTe thermoelectric inks for 3D printing of power-generating tubes *Adv. Energy Mater.* **11** 2100190
[43] Choo S *et al* 2021 Cu_2Se-based thermoelectric cellular architectures for efficient and durable power generation *Nat. Commun.* **12** 3550
[44] Howells G, Mehraban S, McGettrick J, Lavery N, Carnie M J and Burton M 2023 Rapid printing of pseudo-3D printed SnSe thermoelectric generators utilizing an inorganic binder *ACS Appl. Mater. Interfaces* **15** 23068–76
[45] Pei J, Cai B, Zhuang H-L and Li J-F 2020 Bi_2Te_3-based applied thermoelectric materials: research advances and new challenges *Natl Sci. Rev.* **7** 12
[46] Saberi Y and Sajjadi S A 2022 A comprehensive review on the effects of doping process on the thermoelectric properties of Bi_2Te_3 based alloys *J. Alloys Compd.* **904** 163918
[47] Chang P, Mei H, Zhou S, Dassios K G and Cheng L 2019 3D printed electrochemical energy storage devices *J. Mater. Chem.* A **7** 4230
[48] Kim F *et al* 2021 Direct ink writing of three-dimensional thermoelectric microarchitectures *Nat. Electron.* **4** 579–87
[49] Ahn B Y, Duoss E B, Motala M J, Guo X, Park S-I, Xiong Y, Yoon J, Nuzzo R G, Rogers J A and Lewis J A 2009 Omnidirectional printing of flexible, stretchable, and spanning silver microelectrodes *Science* **323** 1590–3
[50] Duty C, Ajinjeru C, Kishore V, Compton B, Hmeidat N, Chen X, Liu P, Hassen A A, Lindahl J and Kunc V 2018 What makes a material printable? A viscoelastic model for extrusion-based 3D printing of polymers *J. Manuf.* **35** 526–37
[51] Eom Y, Kim F, Yang S E, Son J S and Chae H G 2019 Rheological design of 3D printable all-inorganic inks using BiSbTe-based thermoelectric materials *J. Rheol.* **63** 291–304
[52] Su N, Zhu P, Pan Y, Li F and Li B 2020 3D-printing of shape-controllable thermoelectric devices with enhanced output performance *Energy* **195** 116892
[53] Kenel C, Al Malki M M F and Dunand D C 2021 Microstructure evolution during reduction and sintering of 3D-extrusion-printed $Bi_2O_3+TeO_2$ inks to form Bi_2Te_3 *Acta Mater.* **221** 117422
[54] Yang S E *et al* 2021 Composition-segmented BiSbTe thermoelectric generator fabricated by multimaterial 3D printing *Nano Energy* **81** 105638
[55] Zhang D *et al* 2023 3D-printed porous thermoelectrics for in situ energy harvesting *ACS Energy Lett.* **8** 332–8
[56] Ana L P *et al* 2019 Printed flexible μ-thermoelectric device based on hybrid Bi_2Te_3/PVA composites *ACS Appl. Mater. Interfaces* **11** 9
[57] Madan D, Chen A, Wright P K and Evans J W 2012 Printed Se-doped MA n-type Bi_2Te_3 thick-film thermoelectric generators *J. Electron. Mater.* **41** 1481–6
[58] Chen A, Madan D, Wright P K and Evans J W 2011 Dispenser-printed planar thick-film thermoelectric energy generators *J. Micromech. Microeng.* **21** 104006
[59] Chen A, Madan D, Koplow M, Wright P K and Evans J W 2009 Dispenser printed thermoelectric energy generators *PowerMEMS*
[60] Saadi M A S R, Maguire A, Pottackal N T, Thakur M S H, Ikram M M, Hart A J, Ajayan P M and Rahman M M 2022 Direct ink writing: a 3D printing technology for diverse materials *Adv. Mater.* **34** 2108855
[61] Vyavahare S, Teraiya S, Panghal D and Kumar S 2019 Fused deposition modelling: a review *Rapid Prototyp. J.* **26** 176–201
[62] Dhinakaran V, Kumar K P M, Ram P M B, Ravichandran M and Vinayagamoorthy M 2020 A review on recent advancements in fused deposition modeling *Mater. Today: Proc.* **27** 752–6
[63] Penumakala P K, Santo J S A and Thomas A 2020 A critical review on the fused deposition modeling of thermoplastic polymer composites *Composites* B **201** 108336
[64] Du Y, Chen J, Meng Q, Xu J, Lu J, Paul B and Eklund P 2020 Flexible thermoelectric double-layer inorganic/organic composites synthesized by additive manufacturing *Adv. Electron. Mater.* **6** 2000214
[65] Wang J, Li H, Liu R, Li L, Lin Y-H and Nan C-W 2018 Thermoelectric and mechanical properties of PLA/$Bi_{0.5}Sb_{1.5}Te_3$ composite wires used for 3D printing *Compos. Sci. Technol.* **157** 1–9
[66] Du Y, Chen J, Meng Q, Xu J, Paul B and Eklund P 2020 Flexible ternary carbon black/Bi_2Te_3 based alloy/polylactic acid thermoelectric composites fabricated by additive manufacturing *J. Materiomics* **6** 293–9

[67] Oztan C, Ballikaya S, Ozgun U, Karkkainen R and Celik E 2019 Additive manufacturing of thermoelectric materials via fused filament fabrication *Appl. Mater. Today* **15** 77–82
[68] Singh R *et al* 2020 Powder bed fusion process in additive manufacturing: an overview *Mater. Today: Proc.* **26** 3058–70
[69] Ladani L and Sadeghilaridjani M 2021 Review of powder bed fusion additive manufacturing for metals *Metals* **11** 1391
[70] Dejene N D and Lemu H G 2023 Current status and challenges of powder bed fusion-based metal additive manufacturing: literature review *Metals* **13** 424
[71] Hu Q, Luo D, Guo J and Qiu W 2023 3D printing of Bi_2Te_3-based thermoelectric materials with high performance and shape controllability *ACS Appl. Mater. Interfaces* **15** 38623–32
[72] Mao Y, Yan Y, Wu K, Xie H, Xiu Z, Yang J, Zhang Q, Uher C and Tang X 2017 Non-equilibrium synthesis and characterization of n-type $Bi_2Te_{2.7}Se_{0.3}$ thermoelectric material prepared by rapid laser melting and solidification *RSC Adv.* **7** 21439–45
[73] Shi J, Chen X, Wang W and Chen H 2021 A new rapid synthesis of thermoelectric Sb_2Te_3 ingots using selective laser melting 3D printing *Mater. Sci. Semicond.* **123** 105551
[74] El-Desouky A, Carter M, Mahmoudi M, Elwany A and LeBlanc S 2017 Influences of energy density on microstructure and consolidation of selective laser melted bismuth telluride thermoelectric powder *J. Manuf. Process.* **25** 411–7
[75] Zhang H, Hobbis D, Nolas G S and LeBlanc S 2018 Laser additive manufacturing of powdered bismuth telluride *J. Mater. Res.* **33** 4031–9
[76] Wu K, Yan Y, Zhang J, Mao Y, Xie H, Yang J, Zhang Q, Uher C and Tang X 2017 Preparation of n-type Bi_2Te_3 thermoelectric materials by non-contact dispenser printing combined with selective laser melting *Phys. Status Solidi* RRL **11** 6
[77] Shi J, Chen H, Jia S and Wang W 2019 3D printing fabrication of porous bismuth antimony telluride and study of the thermoelectric properties *J. Manuf. Process.* **37** 370–5
[78] Xiong X, Zhu L, Wang G, Liu D, Zhang Q and Feng W 2020 Microstructure and properties of n-type Bi_2Te_3-based thermoelectric material fabricated by selective laser sintering *Mater. Res. Express* **7** 066504
[79] Kruth J-P, Mercelis P, Vaerenbergh J V, Froyen L and Rombouts M 2005 Binding mechanisms in selective laser sintering and selective laser melting *Rapid Prototyp. J.* **11** 26–36
[80] Yadroitsev I and Smurov I 2010 Selective laser melting technology: from the single laser melted track stability to 3D parts of complex shape *Phys. Proc.* **5** 551–60
[81] Olakanmi E O, Cochrane R F and Dalgarno K W 2015 A review on selective laser sintering/melting (SLS/SLM) of aluminium alloy powders: processing, microstructure, and properties *Prog. Mater. Sci.* **74** 401–77
[82] Xie W, Zhang X, Leighton C and Frisbie C D 2017 2D insulator–metal transition in aerosol-jet-printed electrolyte-gated indium oxide thin film transistors *Adv. Electron. Mater.* **3** 1600369
[83] Cao C, Andrews J B and Franklin A D 2017 Completely printed, flexible, stable, and hysteresis-free carbon nanotube thin-film transistors via aerosol jet printing *Adv. Electron. Mater.* **3** 170057
[84] Fisher C, Skolrood L N, Li K, Joshi P C and Aytug T 2023 Aerosol-jet printed sensors for environmental, safety, and health monitoring: a review *Adv. Mater. Technol.* **8** 2300030
[85] Gupta A A, Bolduc A, Cloutier S G and Izquierdo R 2016 Aerosol jet printing for printed electronics rapid prototyping. *2016 IEEE Int. Symp. on Circuits and Systems (ISCAS)* pp 866–9
[86] Zeng M and Zhang Y 2019 Colloidal nanoparticle inks for printing functional devices: emerging trends and future prospects *J. Mater. Chem.* A **7** 23301–36
[87] Ou C, Sangle A L, Datta A, Jing Q, Busolo T, Chalklen T, Narayan V and Kar-Narayan S 2018 Fully printed organic–inorganic nanocomposites for flexible thermoelectric applications *ACS Appl. Mater. Interfaces* **10** 19580–7
[88] Saeidi-Javash M, Kuang W, Dun C and Zhang Y 2019 3D conformal printing and photonic sintering of high-performance flexible thermoelectric films using 2D nanoplates *Adv. Funct. Mater.* **29** 1901930
[89] Hollar C *et al* 2020 High-performance flexible bismuth telluride thin film from solution processed colloidal nanoplates *Adv. Mater. Technol.* **5** 2000600
[90] Melchels F P W, Feijen J and Grijpma D W 2010 A review on stereolithography and its applications in biomedical engineering *Biomaterials* **31** 6121–30
[91] Huang J, Qin Q and Wang J 2020 A review of stereolithography: processes and systems *Processes* **8** 1138
[92] Lopes A J, Lee I H, MacDonald E, Quintana R and Wicker R 2014 Laser curing of silver-based conductive inks for in situ 3D structural electronics fabrication in stereolithography *J. Mater. Process. Technol.* **214** 1935–45
[93] Hagiwara T 2001 Recent progress of photo-resin for rapid prototyping, "resin for stereolithography" *Macromol. Symp.* **175** 397–402
[94] Tiwari L, Tang T, Rong J, Shan W, Yang Y and Li X 2022 Thermoelectric material fabrication using mask image projection based stereolithography integrated with hot pressing *J. Mater. Sci. Technol.* **9** 105–13
[95] Wang Z *et al* 2022 Direct ink writing of high-performance Bi_2Te_3-based thermoelectric materials using quasi-inorganic inks and interface engineering *J. Mater. Chem.* A **10** 12921–7
[96] Madan D, Wang Z, Chen A, Juang R, Keist J, Wright P K and Evans J W 2012 Enhanced performance of dispenser printed MA n-type Bi_2Te composite thermoelectric generators *ACS Appl. Mater. Interfaces* **4** 6117–24
[97] Zhang X, Chen J, Zhang H, Zhu P, Wang R, Li F and Li B 2023 Enhanced thermoelectric performance of 3D-printed Bi_2Te_3-based materials via adding Te/Se *J. Materiomics* **9** 328–37
[98] Leonov V 2013 Thermoelectric energy harvesting of human body heat for wearable sensors *IEEE Sens. J.* **13** 2284–91
[99] Siddique A R M, Mahmud S and Heyst B V 2017 A review of the state of the science on wearable thermoelectric power generators (TEGs) and their existing challenges *Renew. Sustain. Energy Rev.* **73** 730–44
[100] Jo S, Cho S, Yang U J, Hwang G-S, Baek S, Kim S-H, Heo S H, Kim J-Y, Choi M K and Son J S 2021 Solution-processed stretchable Ag_2S semiconductor thin films for wearable self-powered nonvolatile memory *Adv. Mater.* **33** 2100066
[101] Prunet G, Pawula F, Fleury G, Cloutet E, Robinson A J, Hadziioannou G and Pakdel A 2021 A review on conductive polymers and their hybrids for flexible and wearable thermoelectric applications *Mater. Today: Phys.* **18** 100402
[102] Haras M and Skotnicki T 2018 Thermoelectricity for IoT—A review *Nano Energy* **54** 461–76
[103] Junior O H A, Maran A L O and Henao N C 2018 A review of the development and applications of thermoelectric microgenerators for energy harvesting *Renew. Sustain. Energy Rev.* **91** 376–3
[104] Tölle F J, Fabritius M and Mülhaupt R 2012 Emulsifier-free graphene dispersions with high graphene content for printed electronics and freestanding graphene films *Adv. Funct. Mater.* **22** 1136–44
[105] Yin L *et al* 2023 Low-temperature sintering of Ag nanoparticles for high-performance thermoelectric module design *Nat. Energy* **8** 665–74